

Local electrical characterization of laser-recorded marks in $\text{Ge}_2\text{Sb}_2\text{Te}_5$ thin films using conductive-tip atomic force microscopy

Chia Min CHANG¹, Cheng Hung CHU², Ming Lun TSENG¹, Hai-Pang CHIANG², Masud MANSURIPUR^{1,3}
and Din Ping TSAI^{1,4,5}

1) Department of Physics, National Taiwan University, Taipei 106, Taiwan
 2) Institute of Optoelectronic Sciences, National Taiwan Ocean University, Keelung 202, Taiwan
 3) College of Optical Sciences, The University of Arizona, Tucson, Arizona 85721, USA
 4) Research Center for Applied Sciences, Academia Sinica, Taipei 115, Taiwan
 5) Instrument Technology Research Center, National Applied Research Laboratories, Hsinchu 300, Taiwan

<masud@optics.arizona.edu>

Abstract. Local electrical conductivity of $\text{Ge}_2\text{Sb}_2\text{Te}_5$ thin films deposited on a thin-film gold electrode is measured over a fairly large surface area using a conductive-tip atomic force microscope (C-AFM). Being amorphous, the as-deposited chalcogenide films have negligible electrical conductivity. With the aid of a focused laser beam, however, we have written on these films micron-sized crystalline marks, ablated holes surrounded by crystalline rings, and other multi-ring structures containing both amorphous and crystalline zones. Within these structures, nano-scale regions of superior conductivity have been mapped and probed using our high-resolution, high-sensitivity C-AFM. When the $\text{Ge}_2\text{Sb}_2\text{Te}_5$ layer is sufficiently thin, and when laser crystallization/ablation is used to define long, isolated amorphous stripes on the samples, we find the C-AFM-based method of extracting information from the recorded marks to be superior to other forms of microscopy for this particular class of materials. Given the tremendous potential of chalcogenides as the leading media candidates for high-density electronic memories, our method of conductivity enhancement using isolated stripes could be a valuable tool in furthering research and development efforts in this important area of modern technology.

Keywords: Optical recording; recording materials; materials and process characterization.

1. Introduction. Optical and thermal properties of GeSbTe-based phase-change alloys have been used in the past two decades for write-once as well as rewritable optical disk data storage [1-10]. In more recent years, research and development efforts have been directed toward phase-change electronic memories, which exploit the reversible electrical properties of the same class of materials [11-24]. In the context of the latter application, understanding and optimizing the material properties at nano-scale require tools and techniques that are sensitive to changes in the electrical conductivity of the material on the scale of individual crystalline grains, typically only a few nanometers in diameter [25, 26]. Conventional methods of atomic force microscopy, combined with scanning and transmission electron microscopy, provide valuable information about the morphology, crystal structure and orientation, and local composition of the materials. However, local electrical conductivity of the material can only be monitored with scanning probe microscopy using a conductive tip [27-31].

In this paper we use conductive-tip atomic force microscopy (C-AFM) to examine the electrical properties of laser-written marks on as-deposited amorphous $\text{Ge}_2\text{Sb}_2\text{Te}_5$ thin films. We explore the electrical conductivity of various zones within the recorded marks, as well as their dependence on the recording conditions. Isolated narrow stripes carved on the surface of GST thin films will be shown to have superior characteristics for imaging recorded marks at high resolution, enhanced image contrast, and with a high signal-to-noise ratio.

2. Experimental setup. Two sets of thin film stacks on glass substrates, one having the structure ZnS-SiO_2 (130nm)/ $\text{Ge}_2\text{Sb}_2\text{Te}_5$ (10nm), the other being ZnS-SiO_2 (130nm)/Au (5nm)/ $\text{Ge}_2\text{Sb}_2\text{Te}_5$ (10nm), were fabricated using conventional magnetron sputtering equipment (Shibaura Co., Japan). The as-deposited $\text{Ge}_2\text{Sb}_2\text{Te}_5$ films were in the amorphous state; hereinafter, we shall refer to this material as the recording layer. The ZnS-SiO_2 layer, used in the phase-change optical disk industry as the standard under-layer (and also over-layer), is valued for its optical and thermal properties, as well as for its protection of the GST film from undesirable environmental effects. We use the gold (Au) film primarily as an electrically conductive electrode, placing it in direct contact with the GST film. Despite its extreme thinness, the high-thermal-conductivity gold layer will influence, perhaps to a small extent, the formation and properties of the marks written onto the adjacent GST layer. Of the two aforementioned stacks, the one without a gold layer will be our benchmark sample, used to demonstrate that no electrical signals can be detected in the absence of the gold electrode. The sample with 5 nm of gold directly beneath the 10 nm GST layer will be seen to be the one that yields high-contrast C-AFM images of the recorded marks. We mention in passing that we have also experimented with thicker GST films (50 nm and 20 nm) in conjunction with both thin and thick gold films; however, the C-AFM images of recorded marks on these thicker samples were unsatisfactory in all cases. We are thus led to believe that the combination of a 10 nm GST film and a 5 nm gold electrode is nearly ideal for such studies as reported in the present paper.

The laser irradiation of the as-deposited amorphous GST films were carried out using an optical pump-probe system (Static Media Tester, TOPTICA Co., Germany). This system focuses a red laser beam ($\lambda_o = 658$ nm) through a high-numerical-aperture objective lens (NA = 0.65) onto the GST film that is the top layer of our sample. The laser power was controlled in the range from 2.0 mW to 20 mW, while the laser pulse duration could be varied from 100 ns to 1500 ns.

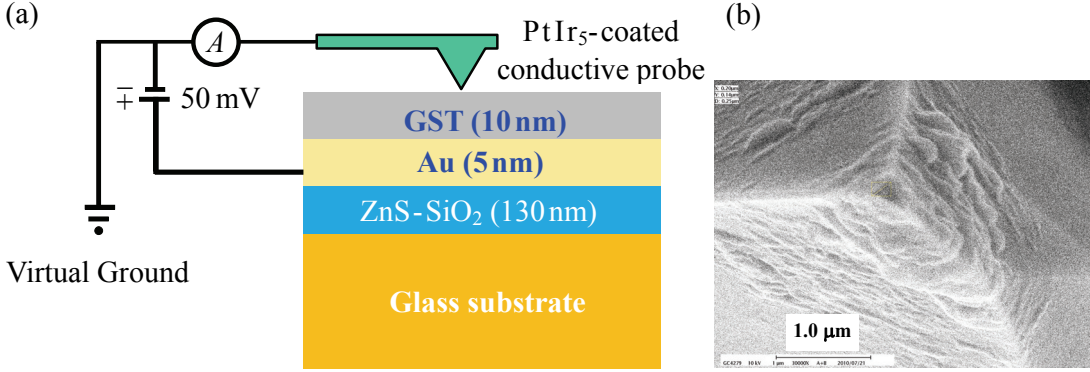


Fig. 1. (a) Diagram of the experimental setup, depicting a conductive-tip AFM measuring the local electric resistivity of a sputter-deposited ZnS-SiO₂(130 nm)/Au(5 nm)/Ge₂Sb₂Te₅(10 nm) stack atop a glass substrate. (b) Scanning electron micrograph of the PtIr₅-coated probe tip.

We examined the morphology as well as the electrical conductivity of recorded marks using an atomic force microscope both with and without its conductive-tip (C-AFM, Asylum Research). The C-AFM cantilever probe is coated with PtIr₅ and is connected to the virtual ground, as shown in Fig. 1(a). A 50 mV bias voltage was applied to the gold film through the application of silver paste and conductive carbon tape to a region of the sample that was about 10 mm away from the area on which various laser-written marks were located. We also used a scanning electron microscope (SEM) equipped with an x-ray diffraction (XRD) micro-probe to analyze the morphology of the recorded marks as well as the concentration of Au within and in the immediate neighborhood of these marks.

3. Results and discussion. Figure 2(a) shows a photo-micrograph of an array of laser-recorded marks on the benchmark sample consisting of amorphous GST film (10nm) and ZnS-SiO₂ under-layer (130nm), coated on a glass substrate. The various laser powers (2.0 mW-20 mW) and pulse durations (100 ns-1500 ns) used in writing these marks are indicated on the vertical and horizontal axes, respectively. It is seen that, at higher laser powers and/or longer pulse durations, the center of the mark will be ablated.

The lower edge of each sample is covered with silver paste, forming the contact pad for the battery during C-AFM measurements. The diagram in Fig. 2(b) shows the patch of silver paste and its distance from the recorded marks (tens of microns). Later, when we write straight lines onto the GST film to create isolated stripes for the recording of marks, the lines will be made long enough to contact the silver paste.

Fig. 2. (a) Reflection optical image of laser-recorded marks on a sample of Glass/ZnS-SiO₂(130 nm)/GST(10 nm), using different laser powers, 2 mW-20 mW, indicated on the vertical axis, and pulse durations, 100 ns-1500 ns, indicated on the horizontal axis. (b) The lower edge of the sample is covered with silver paste, which makes contact with the gold underlayer and creates a return path for the electric current.

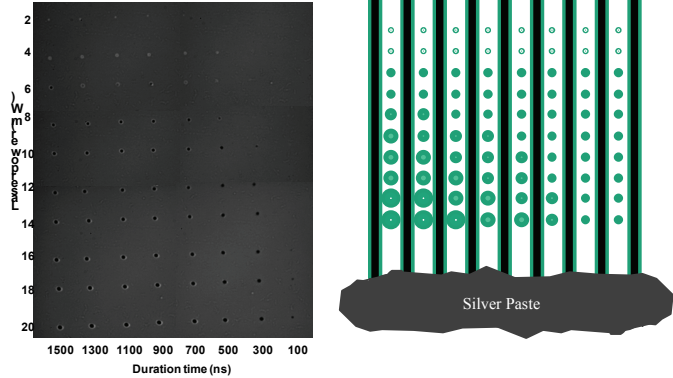


Figure 3(a) is an Atomic Force Microscope (AFM) image of marks recorded on the benchmark sample (same marks as those shown in Fig. 2). The range of laser powers and pulse durations used in this case is 6 mW-20 mW and 100 ns-1500 ns, respectively. The ablated holes are seen to be ~10 nm deep, which is the thickness of the GST layer. These holes are surrounded by a ring whose height is nearly 20 nm above the surface of the sample. Figure 3(b) shows the C-AFM image of the same region of the sample as depicted in Fig. 3(a), with the current gain factor set to 20 nA/V. Hardly any current flows through the sample in this case and, therefore, no images of the recorded marks have been captured.

A close-up view of the mark recorded on the benchmark sample with an 18 mW-1300 ns laser pulse is shown in Fig. 4. The AFM image in Fig. 4(a) and its corresponding cross-sectional view show the raised boundary, the ablated ring immediately inside the raised boundary, and accumulated debris near the center of the mark. The C-AFM image of the same mark shown in Fig. 4(b) is obtained with the current gain factor set to 20 nA/V. A weak current (peak value ~0.7 nA) is seen to flow through the boundary region of the recorded mark. In the absence of a gold under-layer in this sample, the origin of the observed current is uncertain, although, in all likelihood, it is an undesirable consequence of the cross-talk between the AFM tip and the C-AFM electronics.

Fig. 3. (a) AFM image of marks recorded on the benchmark sample of Glass substrate/ZnS- SiO_2 (130nm)/GST (10nm) with different laser powers and pulse durations (6-20 mW, 100- 1500 ns). (b) C-AFM image of the same region of the sample as in (a), monitored under $V_{\text{bias}} = 50$ mV and a current gain of 20 nA/V. No images of the recorded marks have been captured, as no current flows in the absence of the gold electrode.

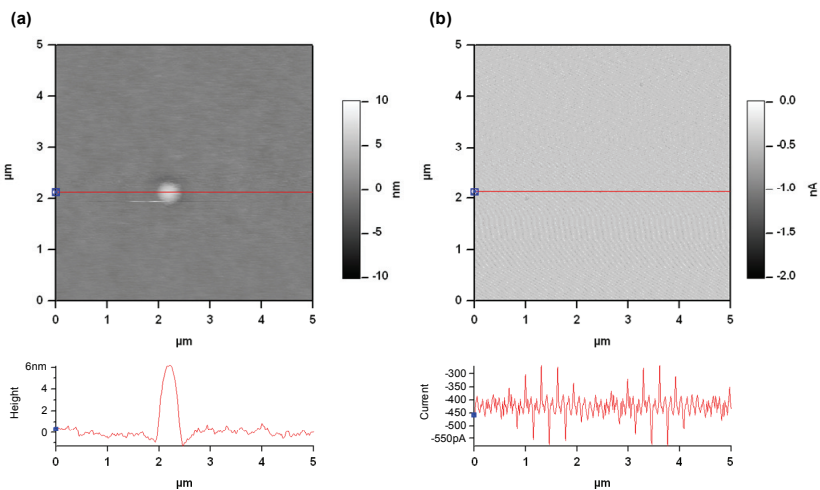
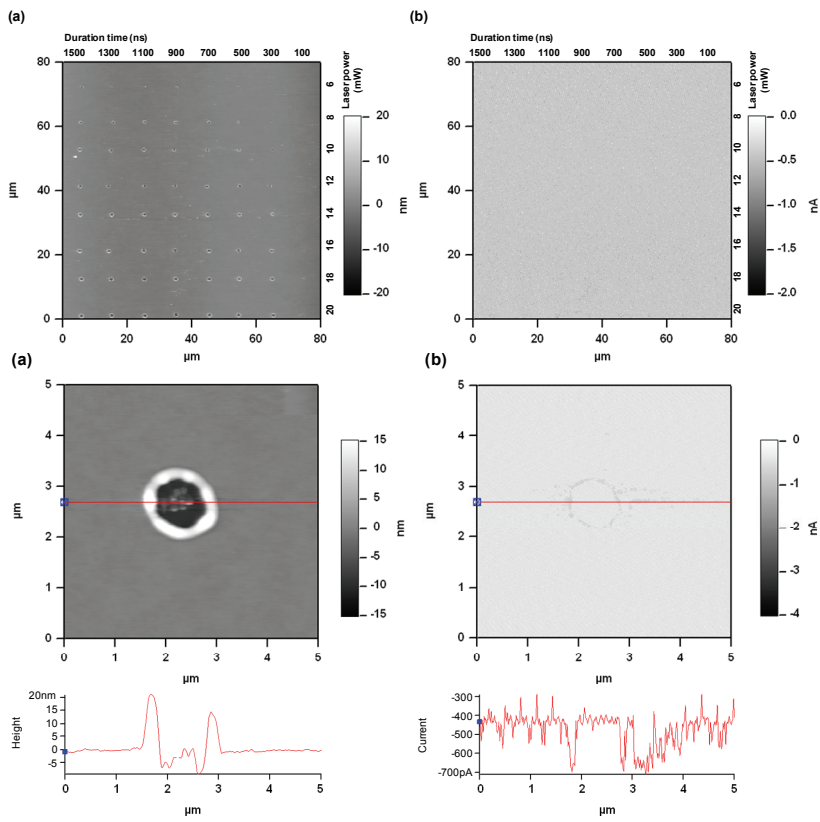
Fig. 4. Close-up view of the mark recorded on the benchmark sample with an 18 mW-1300 ns laser pulse. (a) AFM image and its corresponding cross-sectional profile show the raised ring at the boundary, the ablated region immediately inside the ring, and accumulated debris at the center of the mark. (b) C-AFM image of the mark and its corresponding cross-sectional profile, acquired with the current gain set to 20 nA/V. A weak current, peaking at ~ 0.7 nA and possibly related to the cross-talk between the AFM tip and the C-AFM electronics, is seen to flow through the boundary region of the ablated mark.

Figure 5 is similar to Fig. 4, except that it depicts a mark recorded with a 4.0 mW-1300 ns laser pulse. There is no ablation in this case, and the center of the mark is seen to have risen by about 6.0 nm above the surface of the sample, while the region surrounding the central bump is depressed by about 1.0 nm. As before, the C-AFM signal shown in Fig. 5(b), with its extremely weak electric current peaking at ~ 0.5 nA, is probably due to noise and cross-talk.

Fig. 5. Similar to Fig. 4, but for a mark recorded with a 4.0 mW-1300 ns pulse. The center of the mark is seen in the AFM image in (a) to have risen by about 6.0 nm above the surface of the sample, while the region surrounding the central bump is depressed by ~ 1.0 nm. In the absence of the gold electrode, the extremely weak C-AFM signal in (b), peaking at ~ 0.5 nA and obtained with the gain-factor set to 20 nA/V, is due to noise and cross-talk.

The AFM image of recorded marks on a sample of Glass /ZnS- SiO_2 (130 nm)/Au (5 nm)/GST (10 nm) with different laser powers and pulse durations (6-20 mW, 100-1500 ns) is shown in Fig. 6(a). As before, the marks recorded with a high laser power and/or with long pulses are ablated at the center and exhibit a raised ring at their periphery. The C-AFM image of the same region of the sample, monitored with a current gain of 2.0 nA/V, is shown in Fig. 6(b). The recorded marks are now clearly visible in the C-AFM image, especially within the ring regions of the high-power/long pulse marks.

The AFM close-up image of a mark recorded with an 18 mW-1300 ns laser pulse, depicted in Fig. 7(a), shows that the ablated region is nearly 15 nm deep, that is, both GST and Au have evaporated out of this region. The bright spot at the center of the ablated pit is probably a mixture of GST and Au, but because it is disconnected from the rest of the gold film, it cannot produce any C-AFM signal. The raised boundary of the mark is 15 nm above the surface on the left edge of the ablated hole, and 10 nm on the right edge. The C-AFM image of this mark and its corresponding cross-sectional profile, shown in Fig. 7(b) were obtained with the current gain factor set to 2.0 nA/V. Certain spots within the raised boundary of



the mark conduct electricity, with a current that is as large as 10 nA in some regions. Two possibilities exist for the occurrence of electrical conductivity within the raised ring: (i) the GST film has crystallized and the crystalline grains extend through the thickness of the ring and make contact with the underlying gold film; (ii) ablated gold from the interior regions of the mark is mixed in with GST, producing in certain spots an electrical pathway from the top of the ring to the underlying gold electrode. Without further information, we cannot decide which mechanism is responsible for the observed C-AFM signal within the ring.

Fig. 6. (a) AFM image of recorded marks on a sample of Glass/ZnS-SiO₂ (130 nm)/Au (5 nm)/GST (10 nm), using different laser powers (6 mW-20 mW) and pulse durations (100 ns-1500 ns). (b) C-AFM image of the same region of the sample as in (a), monitored with a gain factor of 2nA/V.

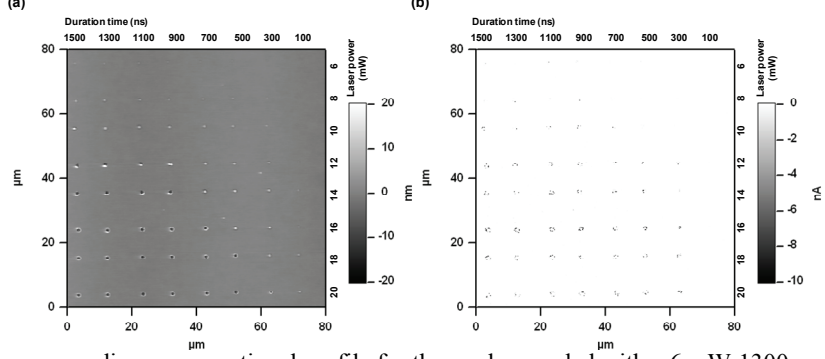


Figure 8(a) is the AFM image and its corresponding cross-sectional profile for the mark recorded with a 6 mW-1300 ns laser pulse within the 10 nm-thick GST film that is in direct contact with the 5 nm-thick gold electrode. The image indicates that the mark consists of a raised core and a slightly depressed boundary. No ablation has taken place, and we suspect the gold film to have remained intact. In all likelihood, the raised core of the mark in the GST layer is detached from the underlying gold film. The slightly depressed, darker ring surrounding the core of the mark is expected to be partially crystalline. The C-AFM image of this mark, shown together with its cross-sectional profile in Fig. 8(b), were obtained with the current gain factor set to 2.0 nA/V. Only the boundary of the recorded mark is seen to be electrically conductive at several spots, with the current being as large as 2.0 nA in some regions. These spots are expected to be crystallites that span the thickness of the GST film and make contact with the Au layer.

Fig. 7. (a) AFM image of a mark recorded with an 18 mW-1300 ns pulse on the GST film. The bright spot at the center of the ablated pit is probably a mixture of GST and Au, but because it is disconnected from the rest of the gold film, it does not produce any C-AFM signal. (b) The C-AFM image and its corresponding cross-sectional profile obtained with the gain-factor set to 2.0 nA/V. Certain spots within the raised boundary of the mark conduct electricity, with the current being as large as 10 nA in some regions.

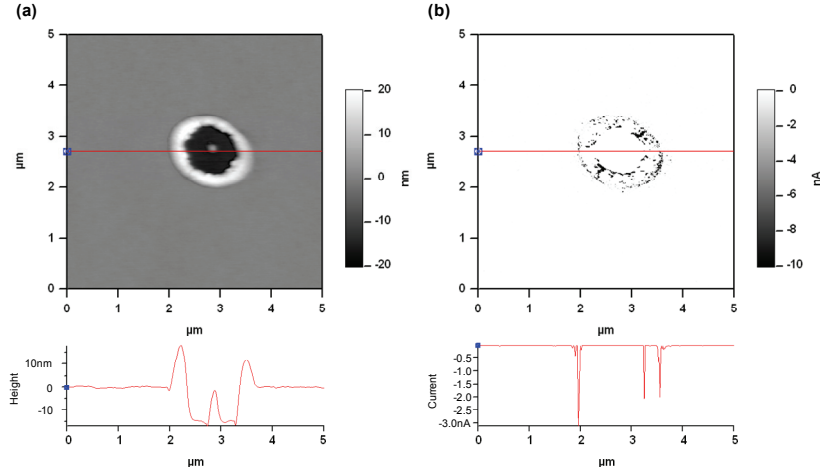


Figure 9(a) is a photo-micrograph of marks recorded with different laser powers and pulse durations (2-20 mW, 100-1500 ns) on the 10 nm-thick GST film deposited atop a 5 nm gold layer. Also recorded on this sample – in the continuous illumination mode – are parallel straight lines written with a cw laser power of 10 mW and a stage velocity of 100 μm/s. The straight lines are ablated, and the gold has been evaporated from the bottom of the grooves. A scanning electron microscope (SEM) image of the same sample is shown in Fig. 9(b). Marks written at low laser power and with short pulse durations are hardly visible in either image.

Figure 10(a) shows an AFM image of recorded marks as well as straight lines in a region of the sample also depicted in Fig. 9. The ranges of the laser pulse power and duration are 6.0-20 mW and 100-1500 ns, respectively. Note that the boundaries of the ablated marks as well as those of the straight lines are raised above the background surface by several nanometers. The C-AFM image of the same region of the sample, acquired with the current gain factor set to 1.0 nA/V, is shown in Fig. 10(b). The boundaries of the ablated lines are highly conductive (current ~ 10 nA), as are those of the ablated marks recorded at high power and/or with long pulses. Also conductive are marks recorded at low laser power with short laser pulses. Marks that are nearly impossible to find in the optical, AFM, and SEM images, are clearly visible in this C-AFM image.

Figure 11(a) is the close-up AFM image and its corresponding cross-sectional profile of a mark recorded with a 18.0 mW-1300 ns laser pulse on an isolated stripe created by the laser-ablated straight lines depicted in Figs. 9 and 10. The boundary of the mark is seen to have risen by as much as 10 nm above the background surface. The interior of the mark is ablated, with both the GST and the gold layers removed from the top of the dielectric under-layer. In the C-AFM image of

the same mark shown in Fig. 11(b), a fairly strong electric current flows through the raised ring surrounding the ablated hole – the current is as large as 9 nA in some regions. Note that the background material, which lacked electrical conductivity in previous examples, is now showing spotty conductivity in what appears to be random locations. The striping of the GST film in the present case must have created alternative paths for current flow which were not previously available.

Fig. 8. (a) AFM image and its corresponding cross-sectional profile indicate that a mark, recorded with a 6 mW-1300 ns pulse on a 10 nm-thick GST film, consists of a raised core and a slightly depressed boundary. (b) C-AFM image of the mark acquired with the current gain factor set to 2.0 nA/V. Only the mark boundary is electrically conductive at several spots, with the current being as large as 2.0 nA in some regions.

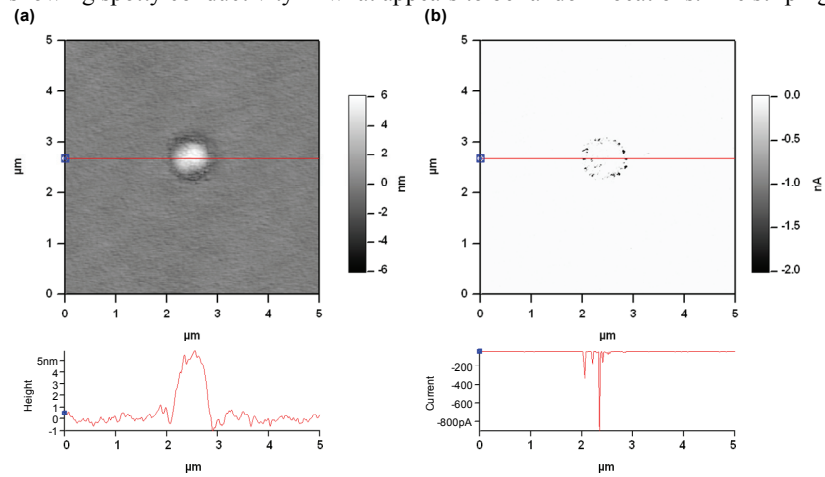


Fig. 9. (a) Reflection optical micrograph of marks recorded with different laser powers/pulse durations (2 mW-20 mW, 100 ns-1500 ns) on the sample having the stack structure Glass/ZnS-SiO₂ (130nm)/Au (5nm)/Ge₂Sb₂Te₅ (10nm). Also written on this sample are straight parallel lines with a cw laser power of 10 mW and a stage velocity of 100 μm/s. The straight lines are ablated and the gold has been evaporated from the bottom of the grooves. (b) SEM image of the same region of the sample as in (a). Marks written at low laser power and with short pulse durations are hardly visible in either image.

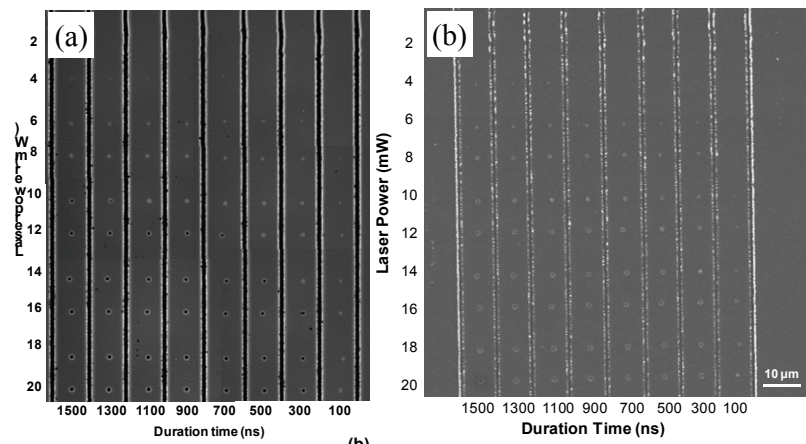


Fig. 10. (a) AFM image of recorded marks and straight lines in a region of the sample also depicted in Fig. 9. The ranges of the laser pulse power and pulse duration are 6.0 mW-20 mW and 100 ns-1500 ns, respectively. (b) C-AFM image of the same region of the sample as in (a), acquired with the current gain factor of 1.0 nA/V.

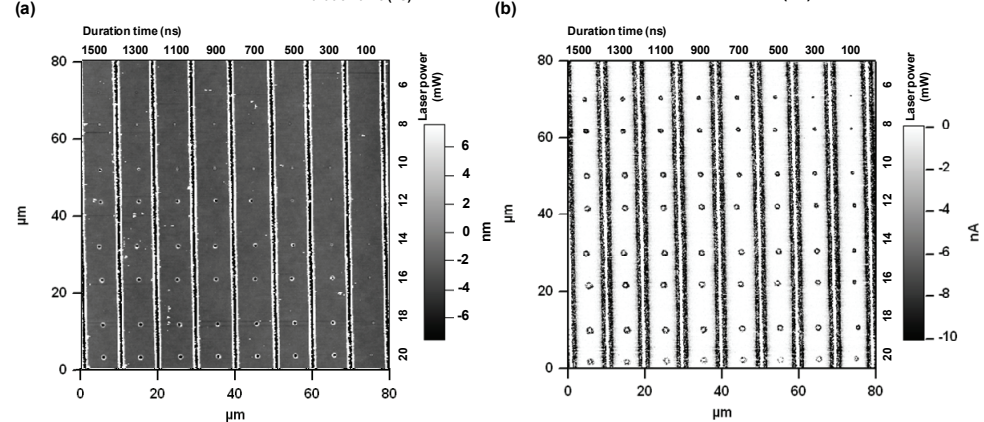


Figure 12(a) is the AFM image of a mark recorded with a 4.0 mW-1300 ns laser pulse on an isolated stripe created by the laser-ablated straight lines depicted in Figs. 9 and 10. The mark is depressed by about 1.5 nm below the surface, a sign that the recorded mark is crystalline. The C-AFM image in Fig. 12(b) shows a spotty current profile in the depressed (crystalline) region and its immediate surroundings, with a current that is often as high as 10 nA. In the optical, SEM, and AFM images, this mark is barely visible, but the C-AFM image is clear and has a good contrast. Note on the right-hand side of Fig. 12(b) how the boundary of the straight-line adjacent to the mark is coming into view.

In Fig. 13(a), the mark recorded with a 4.0 mW-300 ns laser pulse on an isolated stripe of the 10 nm-thick GST film is not visible in the AFM image, but can be seen clearly as an aggregate of dark spots in the C-AFM image depicted in Fig. 13(b). Similarly, the mark recorded with a 6.0 mW-100 ns laser pulse on the same (striped) GST film is not visible in the AFM image of Fig. 14(a), but can be recognized, albeit faintly, in the collection of dark spots in the C-AFM image of Fig. 14(b).

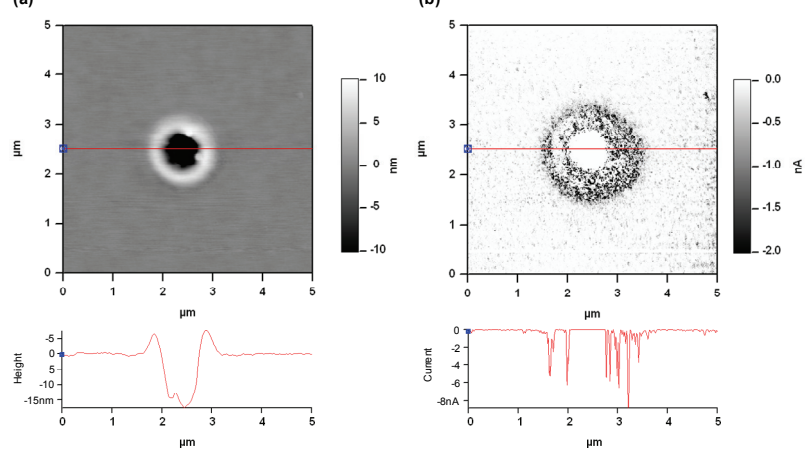


Fig. 11. (a) AFM image of a mark recorded with a 18.0 mW-1300 ns laser pulse. (b) The C-AFM image and its corresponding cross-sectional profile ($V_{bias} = 50$ mV, gain factor = 1.0 nA/V) show a strong electric current – as large as 9 nA in some regions – flowing through the raised ring surrounding the ablated hole.

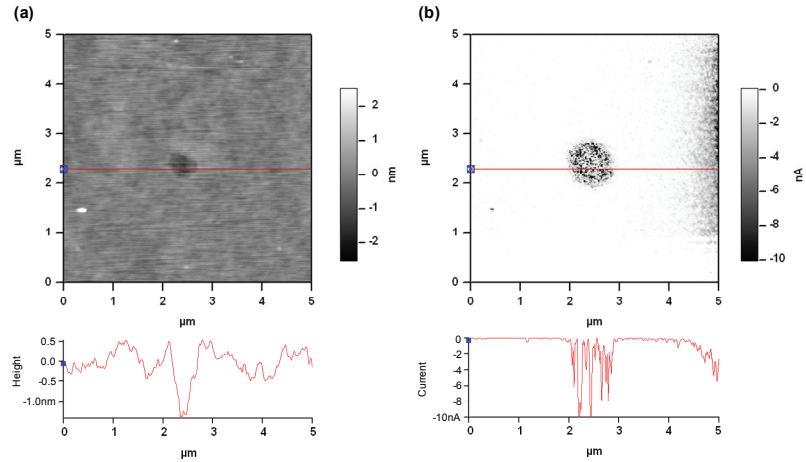


Fig. 12. (a) AFM image of a mark recorded with a 4.0 mW-1300 ns laser pulse on an isolated stripe of a 10 nm-thick GST film. (b) C-AFM image of the same mark, acquired with the current gain factor set to 1.0 nA/V.

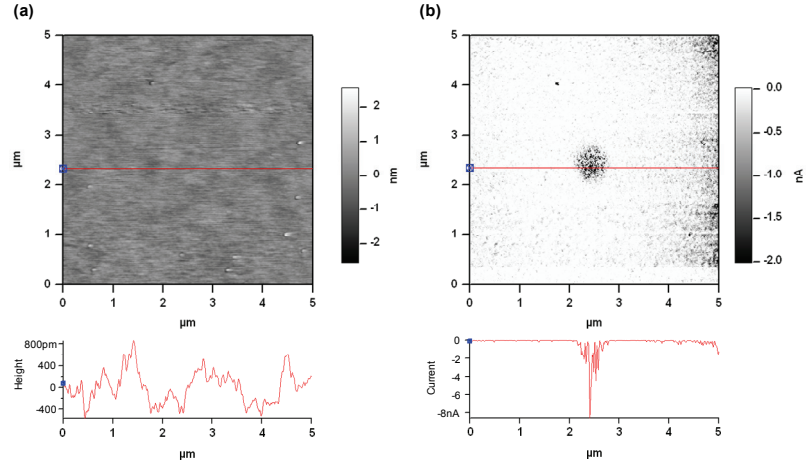


Fig. 13. The mark recorded with a 4.0 mW-300 ns laser pulse is not visible in the AFM image in (a), but can be seen as a collection of dark spots in the C-AFM image in (b). The C-AFM image was recorded with the current gain factor set to 1.0 nA/V.

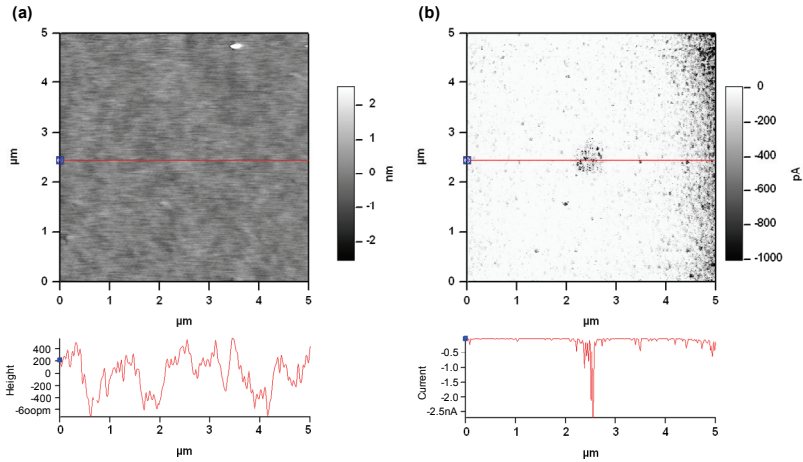


Fig. 14. Mark recorded with a 6.0 mW 100 ns laser pulse is not visible in the AFM image in (a), but can be seen as a faint aggregate of dark spots in the C-AFM image in (b). The C-AFM image was acquired with the current gain factor set to 1.0 nA/V.

4. Summary and conclusions. Conductive-tip atomic force microscopy (C-AFM) is a versatile tool for imaging as well as analyzing the recorded marks in phase-change chalcogenide-based media of data storage. We obtained high-contrast images of laser-written marks on a 10 nm-thick film of amorphous $\text{Ge}_2\text{Sb}_2\text{Te}_5$ that has been sputter-deposited on a 5 nm-thick gold film, which acts as a second electrode for the C-AFM. The image quality and signal-to-noise ratio improved when isolated, 10 μm -wide stripes were created on the GST film by laser ablation of parallel straight lines on the sample.

Although we have reported here only the results of C-AFM microscopy obtained with ablated straight lines, the quality of the images did not suffer at all when the straight lines were written at lower cw laser power (e.g., 2.5 mW rather than 10 mW), thus creating crystalline lines instead of the ablated lines of Figs. 9 and 10. It is likely that regions adjacent to the crystallized or ablated lines, having been exposed to cw irradiation, are more easily crystallized in the process of mark formation, thus producing electrically-conductive filaments throughout the isolated GST stripes, which filaments subsequently form an interconnected network that gives rise to high-contrast C-AFM images of recorded marks.

Acknowledgement. The authors thank the research support from Taiwan's National Science Council under grant numbers 98-2120-M-002-004-, 97-2112-M-002-023-MY2, 99-2811-M-002-003, 96-2923-M-002-002-MY3, 99-2120-M-002-012.

References

1. J. A. Kalb, F. Spaepen, and M. Wuttig, "Kinetics of crystal nucleation in undercooled droplets of Sb- and Te-based alloys used for phase change recording," *J. Appl. Phys.* **98** (2005).
2. D. Lencer, M. Salinga, B. Grabowski, T. Hickey, J. Neugebauer, and M. Wuttig, "A map for phase-change materials," *Nature Materials* **7**, 972-977 (2008).
3. J. Robertson, K. Xiong, and P. W. Peacock, "Electronic and atomic structure of $\text{Ge}_2\text{Sb}_2\text{Te}_5$ phase-change memory material," *Thin Solid Films* **515**, 7538-7541 (2007).
4. M. Wuttig, D. Lusebrink, D. Wamwangi, W. Welnic, M. Gillessen, and R. Dronskowski, "The role of vacancies and local distortions in the design of new phase-change materials," *Nature Materials* **6**, 122-U127 (2007).
5. F. X. Zhai, F. Y. Zuo, H. Huang, Y. Wang, T. S. Lai, Y. Q. Wu, and F. X. Gan, "Optical-electrical properties of AgInSbTe phase change thin films under single picosecond laser pulse irradiation," *J. Non-Crystalline Solids* **356**, 889-892 (2010).
6. S. Shin, H. K. Kim, J. Song, D. J. Choi, and H. H. Cho, "Phase-dependent thermal conductivity of $\text{Ge}_1\text{Sb}_4\text{Te}_7$ and $\text{N:Ge}_1\text{Sb}_4\text{Te}_7$ for phase change memory applications," *J. Appl. Phys.* **107**, 5 (2010).
7. L. P. Shi, T. C. Chong, P. K. Tan, X. S. Miao, J. J. Ho, and Y. J. Wu, "Study of the multi-level reflection modulation recording for phase-change optical disks," *Jpn. J. Appl. Phys. Part 1-Regular Papers Short Notes & Review Papers* **39**, 733-736 (2000).
8. J. Hegedus, and S. R. Elliott, "Microscopic origin of the fast crystallization ability of Ge-Sb-Te phase-change memory materials," *Nature Materials* **7**, 399-405 (2008).
9. W. Welnic, M. Wuttig, S. Botti, and L. Reining, "Local atomic order and optical properties in amorphous and laser-crystallized GeTe," *Comptes Rendus Physique* **10**, 514-527 (2009).
10. M. Wuttig, "Phase-change materials - Towards a universal memory?," *Nature Materials* **4**, 265-266 (2005).
11. W. Welnic and M. Wuttig, "Reversible switching in phase-change materials," *Materials Today* **11**, 20-27 (2008).
12. H. F. Hamann, M. O'Boyle, Y. C. Martin, M. Rooks, and K. Wickramasinghe, "Ultra-high-density phase-change storage and memory," *Nature Materials* **5**, 383-387 (2006).
13. M. H. R. Lankhorst, B. Ketelaars, and R. A. M. Wolters, "Low-cost and nanoscale non-volatile memory concept for future silicon chips," *Nature Materials* **4**, 347-352 (2005).
14. A. Redaelli, A. Pirovano, E. Pellizzer, A. L. Lacaita, D. Ielmini, and R. Bez, "Electronic switching effect and phase-change transition in chalcogenide materials," *IEEE Electron Device Lett.* **25**, 684-686 (2004).

15. W. Welnic, A. Pamungkas, R. Detemple, C. Steimer, S. Blugel, and M. Wuttig, "Unravelling the interplay of local structure and physical properties in phase-change materials," *Nature Materials* **5**, 56-62 (2006).
16. S. H. Lee, Y. Jung, and R. Agarwal, "Highly scalable non-volatile and ultra-lowpower phase-change nanowire memory," *Nature Nanotechnology* **2**, 626-630 (2007).
17. K. Nakayama, M. Takata, T. Kasai, A. Kitagawa, and J. Akita, "Pulse number control of electrical resistance for multi-level storage based on phase change," *J. Phys. D-Applied Physics* **40**, 5061-5065 (2007).
18. D. Krebs, S. Raoux, C. T. Rettner, G. W. Burr, M. Salinga, and M. Wuttig, "Threshold field of phase change memory materials measured using phase change bridge devices," *Applied Physics Letters* **95**, 3 (2009).
19. M. Terao, T. Morikawa, and T. Ohta, "Electrical Phase-Change Memory: Fundamentals and State of the Art," *Jpn. J. Appl. Phys.* **48**, 14 (2009).
20. Y. Jung, S. H. Lee, A. T. Jennings, and R. Agarwal, "Core-shell heterostructured phase change nanowire multistate memory," *Nano Letters* **8**, 2056-2062 (2008).
21. R. Fallica, J. L. Battaglia, S. Cocco, C. Monguzzi, A. Teren, C. Wiemer, E. Varesi, R. Cecchini, A. Gotti, and M. Fanciulli, "Thermal and Electrical Characterization of Materials for Phase-Change Memory Cells," *J. Chem. Eng. Data* **54**, 1698-1701 (2009).
22. Y. Yin, T. Noguchi, H. Ohno, and S. Hosaka, "Programming margin enlargement by material engineering for multilevel storage in phase-change memory," *Applied Physics Letters* **95** (2009).
23. R. E. Simpson, M. Krbal, P. Fons, A. V. Kolobov, J. Tominaga, T. Uruga, and H. Tanida, "Toward the ultimate limit of phase-change in $\text{Ge}_2\text{Sb}_2\text{Te}_5$," *Nano Lett.* **10**, 414-419 (2010).
24. F. X. Zhai, H. Huang, Y. Wang, Y. Q. Wu, and F. X. Gan, "Optical-electrical hybrid operation with amorphous $\text{Ge}_1\text{Sb}_4\text{Te}_7$ phase change thin films," *Applied Physics A - Materials Science & Processing* **98**, 795-800 (2010).
25. G. Bruns, P. Merkelbach, C. Schlockermann, M. Salinga, M. Wuttig, T. D. Happ, J. B. Philipp, and M. Kund, "Nanosecond switching in GeTe phase change memory cells," *Appl. Phys. Lett.* **95**, 3 (2009).
26. I. Friedrich, V. Weidenhof, W. Njoroge, P. Franz, and M. Wuttig, "Structural transformations of $\text{Ge}_2\text{Sb}_2\text{Te}_5$ films studied by electrical resistance measurements," *J. Appl. Phys.* **87**, 4130-4134 (2000).
27. T. Gotoh, K. Sugawara, and K. Tanaka, "Nanoscale electrical phase-change in GeSb_2Te_4 films with scanning probe microscopes," *J. Non-Crystalline Solids* **299**, 968-972 (2002).
28. B. J. Bae, S. H. Hong, S. Y. Hwang, J. Y. Hwang, K. Y. Yang, and H. Lee, "Electrical characterization of Ge-Sb-Te phase change nano-pillars using conductive atomic force microscopy," *Semiconductor Science and Technology* **24** (2009).
29. S. K. Lin, P. Yang, I. C. Lin, H. W. Hsu, and D. P. Tsai, "Resolving nano-scale recording bits on phase-change rewritable optical disk," *Jpn. J. Appl. Phys.* **45**, 1431-1434 (2006).
30. S. K. Lin, I. C. Lin, S. Y. Chen, H. W. Hsu and D. P. Tsai, "Study of nano-scale recorded marks on phase-change recording layers and the interactions with surroundings," *IEEE. Trans. Magnet.* **43**, 861-863 (2007).
31. C. H. Chu, B. J. Wu, T. S. Kao, Y. H. Fu, H-P. Chiang, and D. P. Tsai, "Imaging of recording marks and their jitters with different writing strategy and terminal resistance of optical output," *IEEE. Trans. Magnet.* **45**, 2221-2223 (2009).

Presenter's Biography: Masud Mansuripur (PhD Elec. Eng., Stanford, 1981) is Professor and Chair of Optical Data Storage at the College of Optical Sciences of the University of Arizona in Tucson. A Fellow of the Optical Society of America (OSA) and the Society of Photo Instrumentation Engineers (SPIE), he is the author of "*Introduction to Information Theory*" (Prentice-Hall, 1988), "*The Physical Principles of Magneto-Optical Recording*" (Cambridge Univ. Press, 1995), "*Classical Optics and Its Applications*" (Cambridge Univ. Press, 1st edition 2002, Japanese edition 2006, 2nd expanded English edition 2009), and "*Field, Force, Energy, and Momentum in Classical Electrodynamics*" (Bentham e-books, 2011). Dr. Mansuripur has published over 200 papers in peer-reviewed journals, has given more than 150 invited talks and keynote addresses at national and international forums, is founder and CEO of *MM Research, Inc.*, a developer of simulation software for the optical data storage industry, and has been a member of the technical advisory boards of several U.S., European, and Taiwanese corporations.